Clinical Science: this is an Accepted Manuscript, not the final Version of Record. You are encouraged to use the Version of Record that, when published, will replace this version. The most up-to-date version is available at http://dx.doi.org/10.1042/CS20170004. Please cite using the DOI 10.1042/CS20170004

Vascular basement membrane alterations and β-amyloid accumulations in an animal model of cerebral small vessel disease

Friederike Held[1]*, Alan W.J. Morris[2]*, Daniel Pirici[3], Solveig Niklass[1], Matthew M.G. Sharp[2], Cornelia Garz[1], Anne Assmann[1], Hans-Jochen Heinze[1], Frank Schreiber[1], Roxana Carare[2]* and Stefanie Schreiber[1]*

* equally contributed

[1] Department of Neurology, Otto-von-Guericke University Magdeburg, Germany, German Center for Neurodegenerative Diseases (DZNE), Magdeburg, Germany

[2] Faculty of Medicine, University of Southampton, UK

[3] Department of Research Methodology, University of Medicine and Pharmacy of Craiova, Romania

Number of words: 4054

Number of Figures: 5

Number of Tables: 3

Correspondence to

Stefanie Schreiber
Department of Neurology
Otto-von-Guericke University Magdeburg
German Center for Neurodegenerative Diseases (DZNE)
Leipziger Strasse 44
39120 Magdeburg
Germany
Phone: +49 391 6713431
Fax: +49 391 6715233
Email: stefanie.schreiber@med.ovgu.de

Abstract

Non-amyloid cerebral small vessel disease (CSVD) and cerebral amyloid angiopathy (CAA) may be interrelated by the damaged basement membranes (BMs) and extracellular matrix changes of small vessels, resulting in a failure of β-amyloid (Aβ) transport and degradation. We analysed BM changes and the pattern of deposition of Aβ in the walls of blood vessels in spontaneously hypertensive stroke-prone rats (SHRSP), a non-transgenic CSVD model.

In 45 SHRSP and 38 Wistar rats aged 18 to 32 weeks 1) the percentage area immunostained for vascular collagen IV and laminin was quantified, 2) the capillary BM thickness as well as endothelial and pericyte pathological changes were analysed using transmission electron microscopy (TEM) and 3) the presence of vascular Aβ was assessed.

Compared to controls, SHRSP exhibited a significantly higher percentage area immunostained with collagen IV in the striatum and thalamus. SHRSP also revealed an age-dependent increase of the capillary BM thickness and of endothelial vacuoles (caveolae) within subcortical regions. Endogenous Aβ deposits in the walls of small blood vessels were observed in the cortex (with the highest incidence found within fronto-parietal areas), striatum, thalamus and hippocampus. Vascular β-amyloid accumulations were frequently detected at sites of small vessel wall damage.

Our data demonstrate changes in the expression of collagen IV and of the ultrastructure of BMs in the small vessels of SHRSP. Alterations are accompanied by vascular deposits of endogenous Aβ. Impaired β-amyloid clearance along perivascular and endothelial pathways and failure of

extracellular Aβ degradation may be key mechanisms connecting non-amyloid CSVD and CAA.

***Keywords**:* cerebral small vessel disease, cerebral amyloid angiopathy, spontaneously hypertensive animal model, perivascular Aβ drainage

1. Introduction

Non-amyloid sporadic cerebral small vessel disease (CSVD) and sporadic cerebral amyloid angiopathy (CAA) have been considered as rather distinct vascular pathologies of the ageing brain [1]. CSVD is predominantly characterized by endothelial damage, blood brain barrier (BBB) breakdown and subsequent small vessel wall degeneration, while CAA is mainly characterized by the deposition of amyloid-β (Aβ) in the basement membranes of capillaries and smaller arteries [2, 3]. CSVD and CAA are both related to cognitive decline and are frequently found in various dementia subtypes, comprising those with Alzheimer's disease (AD) neuropathology [4–6].

As identified by transmitted light microscopy and magnetic resonance imaging (MRI), cerebral small vessel wall damage in CSVD and CAA is indicated by microbleeds in the grey matter and by an increased number of enlarged, visible perivascular spaces (PVS) surrounding the arterioles in the basal ganglia or in the white matter [7, 8]. Strictly cortical microbleeds and white matter PVS appear to be associated with CAA, while the combination of microbleeds and PVS in the basal ganglia and in mixed subcortical-cortical locations seems to be more closely related to CSVD [9–11]. Although basal ganglia, cortical and white matter microbleeds and PVS share a common risk profile, including age and arterial hypertension [12–14], their different locations suggest there may be differences between the pathogenic mechanisms underlying CSVD and CAA.

Recent multimodal in vivo imaging data, however, challenged the commonly accepted distinction between CSVD and CAA, reporting an interaction between CSVD load and Aβ burden for the prevalence of cortical microbleeds [15]. Those interactions may be explained by CSVD related inflammatory and degenerative small vessel wall changes also affecting the integrity of the extracellular matrix, vascular basement membranes and endothelium which in turn could lead to a failure of β-amyloid degradation and transport, and thus to CAA development [16]. On the other hand, in CAA, the progressive accumulation of Aβ results in tunica media degeneration and BBB breakdown, resembling closely the changes that occur in CSVD [2, 17]. It thus seems that non-amyloid CSVD and CAA are conditions that appear within the same disease spectrum.

Our study aimed to investigate whether there is an association between CSVD and specific basement membrane and extracellular matrix changes that could underline the relationship between CSVD and CAA. We therefore examined morphological and biochemical alterations of small vessel basement membranes and whether there is any sporadic deposition of Aβ in the walls of blood vessels in spontaneously hypertensive stroke-prone rats (SHRSP), a valid model of non-amyloid cerebral small vessel disease [18].

2. Materials and Methods

2.1. Animals

All animal procedures were conducted after obtaining the approval of the Animal Care Committee of Sachsen Anhalt, Magdeburg, Germany (reference number of license for animal testing 42502-2-1148 DZNE). Animals were obtained from Charles River Laboratories International Inc., Wilmington, MA, USA, housed with a natural light–dark cycle and were allowed to access water and food ad libitum. To record the health status of all animals, neurological function such as decreased spontaneous activity, coordination failure, falling to one side and hunched posture was assessed daily and body weight was monitored weekly.

Overall, 45 male SHRSP and 38 male Wistar rats were included in the study. For histology 19 SHRSP (18 weeks (w) n=6, 24w n=6, 32w n=7) and 14 Wistar rats (18w n=4, 24w n=5, 32w n=5), for collagen IV and laminin immunohistochemistry 15 SHRSP (18w n=5, 24w n=5, 32w n=5) and 15 Wistar rats (18w n=5, 24w n=5, 32w n=5), for STL immunohistochemistry 9 SHRSP (18w n=3, 24w n=3, 32w n=3) and 9 Wistar rats (18w n=3, 24w n=3, 32w n=3), for Aβ-immunohistochemistry 10 SHRSP (18w n=1, 28w n=2, 32w n=7) and for transmission electron microscopy (TEM) 9 SHRSP (18w n=3, 24w n=3, 32w n=3) and 9 Wistar rats (18w n=3, 24w n=3, 32w n=3) were investigated.

For histology and immunohistochemistry, animals were perfused intracardially with phosphate-buffered saline (PBS) and 4% paraformaldehyde (PFA). Brains were fixed in 4% PFA for 48 hours and cryoprotected in 30% sucrose

(6 days); they were then sectioned using a cryostat and coronal brain sections (30 µm thickness) were taken from 11 planes from the frontal to the occipital pole.

For TEM, after perfusion with PBS brains were fixed in a 2%formalin-2.5%gluteralaldehyde-mixture for 48 hours.

2.2. Procedures

2.2.1. General histological assessment

Eleven coronal sections (one section per plane) per animal were stained with Congo red (CR), CR/Prussian blue, Thioflavin S/Prussian blue and Thioflavin T/Prussian blue for the simultaneous detection of dense vascular Aβ accumulations and iron deposits indicative of small vessel wall damage [19].

2.2.2. Immunohistochemistry for basement membrane and endothelial components

For anti-collagen IV and anti-laminin immunohistochemistry 12 coronal sections per animal were stained. In short, sections were incubated in 3% hydrogen peroxide (15 min), incubated in pepsin (1 mg/mL in 0.2N HCL, 4 min, at 37 °C), blocked with 15% normal goat serum (15 min, room temperature), and then incubated overnight either with rabbit anti-rat collagen IV (1:500, Abcam, Cambridge, UK) or with rabbit anti-rat laminin (1:500; Sigma-Aldrich, Dorset, UK) in PBSt (PBS with 0.1% triton) at 4°C. The next day, sections were first incubated with biotinylated goat anti-rabbit IgG in PBSt (1:400, Vector, Peterborough, UK), then incubated with an Avidin-Biotin Complex (ABC) (1:200, 1h, room temperature), and developed using glucose

oxidase Diaminobenzidine (DAB)-nickel enhancement. Photomicrographs were captured using a Leica transmission light microscope and exported to Image J software (NIH, Maryland, USA) for quantification.

For anti-STL immunohistochemistry 3 coronal sections per animal were stained. In short, repeated washing of the slices in PBS and blocking with 0.1 mol/L PBS, 0.5% Triton-X and 10% donkey serum was followed by immunohistochemical staining with solanum tuberosum lectin-fluorescein isothiocyanate (STL-FITC, 1 :500, Axxora, Enzo Life Sciences GmBH, Lörrach, GER) overnight at 4°C in PBS containing 5% donkey serum. Finally DAPI staining (DAPI = 4′.6-Diamidin-2-phenylindol, 1:10000; MoBiTec, Göttingen, GER) was performed for 20 minutes at room temperature. After dehydration with increasing concentrations of alcohol, slices were mounted on slides with Histomount.

2.2.3. Assessment of the presence of endogenous Aβ in SHRSP

Five sections per animal were stained. Sections were pretreated with citrate buffer (70 °C, 30 min), repeatedly washed in PBS, blocked with 10% donkey serum, and subsequently stained with STL-FITC (solanum tuberosum lectin-fluorescein isothiocyanate, endothelial marker, 1:500; Axxora, Enzo Life Sciences GmbH, Lörrach, GER) and rabbit anti-rodent Aβ (1:500; Covance, Dedham, MA, USA) as primaries overnight at 4 °C. Cy5-donkey anti-rabbit IgG (1:500, detection of Aβ; Jackson Immuno Research) was used as secondary antibody for two hours, and DAPI (4'.6-diamidino-2-phenylindol, nuclear staining, 1:10.000; MoBiTec GmbH, Göttingen, GER) staining was performed for 20 min at room temperature. After dehydration with increasing

concentrations of alcohol, sections were mounted on slides with Histomont (Fisher Scientific GmbH, Schwerte, GER).

2.2.4. Transmission electron microscopy for analysis of the ultrastructure of the cerebrovascular basement membranes

Sagittal sections (100 µm) were stored in 0.01M PBS, pH 7.2 until being processed for TEM. Frontoparietal cortex, striatum, hippocampus and thalamus were microdissected and processed as follows: sections were washed in 0.1M phosphate buffer (PB) pH 7.2, post-fixed in osmium tetroxide (1% in 0.1M PB at pH 7.2, 1 hour) and then dehydrated (alcohol series: 30% for 10 min, 50% for 10 min, 70% (in 2% uranyl acetate) for 40 min, 90% overnight and absolute for 2x10 min). Sections were then treated with neat acetonitrile (10 min), immersed in a resin (TAAB Laboratories Equipment, Aldermaston, UK) and acetonitrile mix (50:50) over night, and on the following day treated with fresh neat TAAB resin (6h) before being placed in fresh resin (TAAB Laboratories Equipment, Aldermaston, UK) for polymerization (60°C, 18 hours). Once polymerised, the tissue was sectioned (Leica-Reichert Ultracut E ultra-microtome, Leica, UK), cut into 0.5 µm thick sections, mounted on frosted glass slides and analysed on a Nikon 80i brightfield microscope (Nikon, Japan, x75 magnification) to confirm if the section contained a sufficient amount of capillaries. Ultra-thin transverse sections (90 nm) were prepared and floated on to copper/palladium TEM grids for visualisation of the capillaries. Only cross-sectional capillaries were considered. For quantification images were exported to ITEM software (Olympus, UK). Images were exported to Photoshop CS software (Adobe, UK), for qualitative observations of the structures of the capillary walls.

2.3 Data analysis and quantification

2.3.1. Immunohistochemical assessment of cerebrovascular basement membranes and endothelial components

The relative % signal area of collagen-IV- and laminin-positive capillaries (luminal diameter < 15 µm) and arterioles/small arteries (luminal diameter ≥ 15 µm) [21, 22] was quantified in 6 randomly chosen sections from different brain regions per animal. Analyses were performed separately in the cortex, striatum and thalamus. For each region, 4 randomly selected fields of view (FOVs) per section were quantified using Image J (NIH, Maryland, USA). By setting a threshold for staining intensity and determining the vessel size (< or ≥ 15 µm, see above), we calculated the percentage of coverage of vessels relative to the background per FOV for each region. STL-positive capillaries and arterioles were counted in 10 randomly selected FOVs per animal and region (cortex, striatum, thalamus).

2.3.2. Assessment of endogenous Aβ in SHRSP

The presence of immunocytochemically and histologically detected Aβ deposits in the walls of capillaries (luminal diameter < 15 µm) and arterioles (luminal diameter ≥ 15 µm) was first assessed in a binary manner (existent, not existent). The number of Aβ positive vessels was then counted within 3 FOVs per section using all available sections stained for the assessment of β-amyloid (see above). Cortical, striatal, hippocampal and thalamic regions were analysed.

2.3.3. Analyses of cerebrovascular basement membranes by transmission electron microscopy

Three TEM grids per animal were used for analysis of cortical, striatal, hippocampal and thalamic capillaries defined as having: a luminal diameter of 4.0-15 µm [23], a single endothelial layer with tight junctions and a fused endothelial-astroglial basement membrane. For analysis, 5 transversely orientated capillaries per animal were randomly chosen. To assess the overall vessel structure, those capillaries were imaged first at x9.000. Basement membrane thickness was subsequently determined at x50.000 by taking 20 measurements per capillary along each of the two thinnest points of the capillary wall [20]. We additionally quantified the number of (i) endothelial vacuoles (caveolae), (ii) extensions of the endothelial cells into the lumen ("bridging of the endothelium"), (iii) tight junctions that appear to have lost the normal architecture and (iv) abnormal appearing pericytes.

2.4. Statistical analysis

To determine group differences between SHRSP and Wistar controls, general linear models were conducted with group as independent variable and the following were considered as dependent variables: (i) immunocytochemical collagen IV and laminin relative % signal area, (ii) immunohistochemical STL-positive vessels, (iii) thickness of basement membranes as measured by TEM and (iv) endothelial or pericyte pathologies, that are (a) endothelial vacuoles, (b) "endothelial bridging", (c) open tight junctions and (d) abnormal pericytes, as quantified using TEM *(please see also 2.3.3)*. When the variables (i) to (iv)

(a)-(d) demonstrated a dependency on age, the respective model was adjusted for age.

To address the issue of multiple comparisons, the following p-values were deemed to be significant:

- for collagen IV/laminin/STL data (respectively quantified in 3 regions) $p \leq 0.05/9 = 0.006$
- for basement membrane thickness or endothelial vacuoles or "endothelial bridging" or open tight junctions or abnormal pericytes (respectively quantified in 4 regions) $p \leq 0.05/4 = 0.013$, respectively

3. Results

3.1. Immunohistochemical signal area of collagen IV and laminin

SHRSP exhibited a significant, around 2fold higher cortical, striatal and thalamic percentage area immunostained for collagen IV in vessels with a luminal diameter ≥ 15 µm compared to Wistar controls (**Table 1, Figure 1 & Figure 2**). There were no group differences between SHRSP and Wistar rats for the percentage area immunostained for collagen IV in vessels with a luminal diameter < 15 µm (capillaries) (**Table 1, Figure 1**). Compared to Wistar controls, SHRSP displayed significantly higher numbers of cortical vessels with a luminal diameter ≥ 15 µm (as indicated by STL-positivity). The upregulation of immunostaining for collagen IV observed in the cortical vessels with a luminal diameter ≥ 15 µm in SHRSP was related to vessel density alterations **(Table 2)**. Collagen IV group differences found in striatal and thalamic vessels with a luminal diameter ≥ 15 µm were, however, not associated with changes of vessel density. There were no overall group differences for laminin in any of the regions involved (data not shown).

3.2. Ultrastructural features of basement membranes

The capillary thickness of the basement membrane as measured by TEM software was related to age in SHRSP ($p = 0.004$ for striatum, $p = 0.011$ for hippocampus, $p = 0.001$ for thalamus), but not in Wistar rats (**Figure 1**). Significant age-independent (up to 1.3fold) increases in the capillary basement membrane thickness in SHRSP compared to Wistar rats were observed in the striatum ($p < 0.001$), in the hippocampus ($p < 0.001$) and in the thalamus ($p = 0.004$) (**Table 3 & Figure 1)**. The capillary basement

277 membranes in the cortex of SHRSP were also thicker compared to those in
278 Wistar control rats (p = 0.018, trend-level, **Table 3**).

279 Qualitative morphological changes of the capillary walls were observed in
280 SHRSP and in Wistar controls that is degeneration of pericytes, folding of the
281 tight junctions, accumulation of electron lucent lysosomes or lipofuscin and an
282 increased number of caveolae in endothelial cells and pericytes. Fibrillar
283 structures and electron dense deposits were additionally observed in the
284 thickened BMs **(Figure 3)**.

285 Quantification of endothelial and pericyte pathologies revealed a significant
286 age-related increase of abnormal pericytes within the striatum of the SHRSP
287 (p = 0.004) and a significant age-related decrease of "endothelial bridging"
288 within the Wistar controls' striatum (p = 0.004). Compared to Wistar rats
289 SHRSP displayed significant higher numbers of endothelial vacuoles in the
290 striatum (p = 0.004) and in the hippocampus (p = 0.023, trend-level). On a
291 trend-level SHRSP moreover revealed higher numbers of abnormal cortical
292 pericytes (p = 0.07) when compared to Wistar animals.

293 *3.3. Endogenous vascular β-amyloid deposits in SHRSP*

294 Histological assessment of rodent Aβ revealed that nearly all SHRSP
295 sporadically developed vascular Aβ deposits resembling cerebral amyloid
296 angiopathy: at an age of 18w, 5 out of 6 animals were affected (83%), and
297 from an age of 24w on, 13 out of 13 SHRSP (100%) were affected. Deposits
298 were detected in cortical regions in 100% of the animals (mean number of Aβ-
299 positive vessels/FOV 7.3) with the distribution was as follows: in 83% of the
300 SHRSP vascular β-amyloid accumulations were detected in parietal cortices

(mean/FOV 4.2), while in 56% (mean/FOV 2.5) or 33% (mean/FOV 0.5) they were found in frontal or occipital cortices. Aβ deposits were also observed in the striatum (56%, mean/FOV 1.7), the hippocampus (61%, mean/FOV 1.8) and the thalamus (28%, mean/FOV 1.3). **Figure 4** visualizes the incidence with which Aβ-positive vessels in the respective regions were found in SHRSP. Regional color-coding reflects the percentages of affected rats in the respective regions.

Immunohistological assessment of rodent Aβ revealed CAA in 9 out of 10 SHRSP (90%); all affected animals were at an age of 28w and 32w. In cortical regions, CAA was found in 50%, in the striatum in 40%, in the hippocampus in 90%, and in the thalamus in 50% of all SHRSP. Highest number of CAA-positive vessels was found in the hippocampus, while the striatum displayed the lowest number.

Deposits of Aβ were observed in vessels with a luminal diameter ≥ 15 µm and appearance characteristic of small arteries/arterioles as well as in the walls of capillaries with luminal diameter < 15 µm. All deposits of Aβ were located on the abluminal side of the small vessel walls and not on the endothelial surface (**Figure 5**). Furthermore, these deposits were compact, as determined by the Thioflavin staining (**Figure 5**). Of all Aβ depositing vessels within the whole brain 95% additionally displayed iron accumulations (95% in the cortex, 97% in the striatum, 97% in the hippocampus, 96% in the thalamus) **(Figure 5)**.

None of the Wistar animals exhibited any histologically detectable vascular Aβ accumulations.

4. Discussion

Our analysis revealed a significant age-independent increase in the immunohistochemical signal area of collagen IV in subcortical small arteries/arterioles of spontaneously hypertensive stroke prone rats, compared to Wistar controls. The increased percentage area immunostained for collagen IV in cortical regions was related to an increased number of arterioles/small arteries in SHRSP. The basement membranes of subcortical capillaries in the striatum, thalamus and hippocampus were significantly thicker in aged SHRSP compared to control animals, with the capillary basement membranes of the cortex following the same trend. This increase in thickness of the capillary basement membranes was, however, not explained by a capillary increase of the collagen IV or laminin expression. It was indeed accompanied by qualitative and quantitative alterations of the neurovascular unit comprising higher numbers of (i) subcortical endothelial vacuoles and (ii) abnormal cortical pericytes. Additionally, the hypertensive stroke prone rat developed endogenous capillary and arteriolar/arterial vascular Aβ deposits (CAA), commonly occurring at the abluminal vessel wall side and adjacent to cortical and subcortical small vessel wall damage. One may speculate that CAA development in SHRSP might result from different reasons that are failure of perivascular β-amyloid drainage along the altered basement membranes together with Aβ transport disturbances across the leaking BBB and extracellular matrix protein alterations favouring β-amyloid aggregation [24].

Overall, our results confirm (i) the mutual occurrence of non-amyloid CSVD and CAA, as it is commonly found in the aging brain. Despite CAA was predominantly detectable in (fronto-parietal) cortical regions, subcortical areas such as the basal ganglia or the hippocampus were also frequently affected, which is different from humans. These data moreover suggest that (ii) degenerative capillary basement membrane changes occur as a function of age (in combination with arterial hypertension and CSVD). Underlying mechanisms of overall capillary basement membrane alterations (which were characterized by thickening and structural changes of the neurovascular unit) seem thereby to differ from subcortical arteriolar/arterial basement membrane changes (which were characterized by an increase of the collagen IV expression).

Spontaneous CAA development in a non-transgenic non-amyloid CSVD model suggests that there should be some mechanisms connecting the two small vessel disease entities. The soluble Aβ-protein is eliminated from the brain along the cerebral vascular system by a variety of mechanisms comprising (i) enzymatic degradation, (ii) transport across the blood-brain barrier and (iii) brain-wide lymphatic Aβ-drainage into the extracranial lymphatic system (a) along the vessels' basement membranes or (b) along glial water channels of the glymphatic system [25–27]. All of the mechanisms for the elimination of Aβ depend on the existence of vascular and extracellular matrix integrity, which fails with age, high vascular risk and vessel wall damage, as found in non-amyloid CSVD [26, 27]. Alterations of the Aβ clearance pathways in the cerebral vessel walls caused by BBB breakdown, basement membrane and neurovascular unit damage comprising extracellular

matrix proliferation, result in the accumulation of solutes such as β-amyloid in the small vessel walls. Our findings of extracellular matrix protein and small vessel basement membrane alterations in CSVD along with CAA development, suggest that failure of β-amyloid drainage and degradation may play a crucial role in connecting non-amyloid and amyloid-related CSVD. Failure of perivascular Aβ transport is additionally supported by the observation that in our SHRSP model vascular Aβ was mainly found (i) in the protein clearance pathways at the abluminal side of the small vessel walls and (ii) at sites of small vessel wall damage.

Our results replicate previous findings in the SHRSP and SHR (spontaneously hypertensive rat), namely capillary basement membrane thickening (which depended on age) and the occurrence of qualitative capillary wall changes such as endothelial degeneration [28, 29]. In SHRSP small vessel wall changes are moreover accompanied by structural vascular smooth muscle cell alterations surrounded by many layers of basal lamina-like material of the large arteries, that is e.g. the middle cerebral artery [30]. In the small vasculature, plasma protein leakage (which is commonly found in our experimental CSVD model [18, 22]) related to endothelial damage may thereby be one underlying mechanism explaining the accompanying quantitative capillary basement membrane thickening [31, 32]. The latter has been studied by Fredriksson et al. demonstrating that in SHRSP at BBB leakage sites small vessel wall structures can be replaced by multiple basement membrane layers and bundles of collagen fibrils resulting in small vessel wall thickening and stenosis [28]. Regions without BBB damage, however, seem to be free of any vascular alterations [28]. In our study,

endothelial alterations and BBB breakdown became also evident by chronic (perivascular) iron accumulations (see **Figure 5**). The capillary collagen IV and laminin expression patterns, however, remained unchanged, suggesting that other extracellular matrix proteins may be responsible for the thickening observed.

Our data, however, differ from studies performed by Bailey et al. who did not find differences of the collagen IV percentage area in SHRSP compared to Wistar controls [33]. The authors assessed animals aged 5, 16 and 21 weeks, so overall younger than ours that were 18, 24 and 32 weeks; it thus seems to be very conceivable that collagen IV upregulation accompanies overall vessel wall changes progressing as a function of age in SHRSP [22].

Subcortical arteriolar basement membrane alterations were, however, characterized by an upregulation of collagen IV. One may speculate that the increased expression of arteriolar/arterial collagen IV may result from its reduced degradation [34], or from its increased synthesis [28, 35, 36], which, overall may be explained by hypertension-associated changes of matrix metalloproteases activities, and inflammation within the vessel wall [34]. The latter may also account for regional angiogenesis and associated higher microvessel densities [37] found in our hypertensive rat model. Future studies have to better elucidate the pathomechanisms underlying the different capillary and arteriolar/small artery BM alteration patterns and their relation to age.

Our study confirms the observation that non-transgenic animal models with CSVD and/or arterial hypertension sporadically develop vascular Aβ deposits

[38–40]. Interestingly, the regional distribution of CSVD (for further details see [22]) and CAA in the SHRSP model does not represent the commonly accepted pattern in humans of “mainly subcortical- (and white-matter-) dominant” CSVD and “mainly occipital cortical-dominant” CAA. Instead, in SHRSP, both, non-amyloid CSVD and CAA seem to similarly spread into cortical, especially into fronto-parietal, and subcortical regions. This essential finding might be related to differences of anatomical characteristics of the regional cerebral blood vessels between rodents and humans. In humans, cortical and striatal vessels differ this way that cortical arterioles/arteries are characterized by a layer of leptomeninges that is closely adherent to the wall of the vessel, without a perivascular space, whereas in the basal ganglia there are two such layers, separated by a perivascular space [41]. This suggests that in humans Aβ that is unable to clear efficiently across the endothelium or by perivascular clearance may accumulate in the walls of cortical arteries, but not in the basal ganglia, where (human) CAA is very rare [42]. It is reasonable to assume that regional differences in the anatomy of the walls of the cortical and subcortical arteries may also exist in rodents and this is supported by the higher cortical frequency of vascular Aβ deposits. The quite equal distribution of non-amyloid CSVD and CAA in the SHRSP makes it, however, a promising model for studying the interactions between both types of small vessel disease.

Our findings should be viewed in light of some limitations comprising missing mechanistic links between non-amyloid CSVD and CAA. We can speculate about the possible causes leading to Aβ retention in SHRSP, such as the failure of endothelial transporter functions, which will need to be addressed in

446 future studies. Additionally, we assume that the differences of vascular β-
447 amyloid detection using either histological or immunohistochemical stainings
448 rather result from our quantification approach than from sensitivity issues of
449 the various stainings. This way, that for histology slices covering nearly the
450 whole brain were quantified, while quantification of immunohistochemical data
451 took place using just exemplary slices. Those findings overall show, that the
452 SHRSP strain displays a patchy and heterogeneous distribution of vascular β-
453 amyloid positivity. Evaluation of the whole brain rather than performing
454 regionally circumscribed analysis should thus be considered the gold standard
455 when investigating the vascular β-amyloid status of that rat model.

456 In conclusion, our data confirm the relationship between age, non-amyloid
457 CSVD, arterial hypertension and ultrastructural and biochemical capillary and
458 arteriolar/arterial basement membrane and extracellular matrix changes. They
459 moreover suggest that non-amyloid CSVD and CAA should be considered as
460 part of the same vascular disease spectrum in the ageing brain.

Acknowledgments

This work was supported by a grant of the Romanian National Authority for Scientific Research and Innovation, CNCS – UEFISCDI, project number PN-II-RU-TE-2014-4-0582, contract number 160/01.10.2015. We moreover thank Cheryl A Hawkes for excellent methodological and technical advice.

Conflicts of interest

The authors declare that there are no conflicts of interest.

Tables

Table 1. Collagen IV mean relative % signal area per group and region. SD [standard deviation], SHRSP, spontaneously hypertensive stroke-prone rats, $p \leq 0.006$ was deemed to be significant. The F-ratio demonstrates the explained variance divided by the unexplained variance of the statistical model.

		Wistar, n=15	**SHRSP, n=15**	
Vessels	Region	Mean [SD]	Mean [SD]	F-ratio (p-value)
Collagen IV all vessels	Cortex	2.90 [1.29]	4.40 [3.18]	6.59 (0.013)
	Striatum	2.09 [1.07]	3.39 [2.92]	6.17 (0.016)
	Thalamus	2.32 [1.73]	3.91 [3.48]	5.45 (0.023)
Collagen IV vessels > 15µm	Cortex	3.40 [1.71]	6.67 [3.42]	10.95 **(0.003)**
	Striatum	2.44 [1.42]	5.46 [3.14]	11.51 **(0.002)**
	Thalamus	2.99 [2.28]	6.30 [3.58]	9.46 **(0.005)**
Collagen IV vessels <15µm	Cortex	2.43 [0.37]	2.40 [0.56]	0.21 (0.65)
	Striatum	2.44 [1.42]	1.58 [0.57]	1.52 (0.23)
	Thalamus	1.69 [0.5]	1.60 [0.75]	0.40 (0.53)

474 **Table 2. STL-positivity per group and region.**

475 SD [standard deviation], SHRSP, spontaneously hypertensive stroke-prone
476 rats, $p \leq 0.006$ was deemed to be significant. The F-ratio demonstrates the
477 explained variance divided by the unexplained variance of the statistical
478 model.

		Wistar, n=9	**SHRSP, n=9**	
Vessels	Region	Mean [SD]	Mean [SD]	F-ratio (p-value)
STL-positivity all vessels	Cortex	56.96 [4.47]	58.88 [4.54]	8.18 (0.010)
	Striatum	41.64 [5.48]	45.18 [6.38]	15.88 **(<0.001)**
	Thalamus	40.71 [4.73]	40.30 [4.14]	0.39 (0.5)
STL-positivity vessels > 15µm	Cortex	2.01 [1.00]	3.41 [1.03]	85.89 **(<0.001)**
	Striatum	2.72 [1.15]	3.07 [1.31]	3.52 (0.06)
	Thalamus	2.94 [1.31]	2.91 [1.16]	0.23 (0.60)
STL-positivity vessels <15µm	Cortex	54.94 [4.37]	55.47 [4.46]	0.63 (0.43)
	Striatum	38.92 [5.43]	42.11 [6.06]	13.82 **(<0.001)**
	Thalamus	37.77 [4.49]	37.39 [4.08]	0.35 (0.60)

Table 3. Basement membrane thickness as measured using TEM per group and region. SD [standard deviation], SHRSP, spontaneously hypertensive stroke-prone rats, $p \leq 0.013$ was deemed to be significant. The F-ratio demonstrates the explained variance divided by the unexplained variance of the statistical model. All values are given in nm. TEM = transmission electron microscopy.

		Wistar, n=9	**SHRSP, n=9**	
	Region	Mean [SD]	Mean [SD]	F-ratio (p-value)
Basement membrane thickness in nm	Cortex	52.19 [3.26]	68.14 [17.82]	6.98 (0.018)
	Striatum	51.76 [5.53]	67.22 [10.83]	19.43 **(0.001)**
	Hippocampus	52.93 [4.86]	66.06 [8.25]	22.7 **(< 0.001)**
	Thalamus	51.65 [4.39]	64.22 [10.68]	8.38 **(0.004)**

References

1. Grinberg LT, Thal DR (2010) Vascular pathology in the aged human brain. Acta Neuropathol. 119(3): 277–290
2. Charidimou A, Gang Q, Werring DJ (2012) Sporadic cerebral amyloid angiopathy revisited: recent insights into pathophysiology and clinical spectrum. J. Neurol. Neurosurg. Psychiatry 83(2): 124–137
3. Wardlaw JM, Smith C, Dichgans M (2013) Mechanisms of sporadic cerebral small vessel disease: insights from neuroimaging. Lancet Neurol. 12(5): 483–497
4. Brenowitz WD, Nelson PT, Besser LM et al. (2015) Cerebral amyloid angiopathy and its co-occurrence with Alzheimer's disease and other cerebrovascular neuropathologic changes. Neurobiol Aging 36(10): 2702–2708. doi: 10.1016/j.neurobiolaging.2015.06.028
5. Kester MI, Goos JD, Teunissen CE et al. (2014) Associations between cerebral small-vessel disease and Alzheimer disease pathology as measured by cerebrospinal fluid biomarkers. JAMA Neurol 71(7): 855–862
6. Miwa K, Tanaka M, Okazaki S et al. (2014) Chronic kidney disease is associated with dementia independent of cerebral small-vessel disease. Neurology 82(12): 1051–1057
7. Greenberg SM, Al Shahi SR, Biessels GJ et al. (2014) Outcome markers for clinical trials in cerebral amyloid angiopathy. Lancet Neurol. 13(4): 419–428
8. Wardlaw JM, Smith EE, Biessels GJ et al. (2013) Neuroimaging standards for research into small vessel disease and its contribution to ageing and neurodegeneration. Lancet Neurol. 12(8): 822–838
9. Charidimou A, Meegahage R, Fox Z et al. (2013) Enlarged perivascular spaces as a marker of underlying arteriopathy in intracerebral haemorrhage: a multicentre MRI cohort study. J. Neurol. Neurosurg. Psychiatry 84(6): 624–629
10. Charidimou A, Jaunmuktane Z, Baron JC et al. (2014) White matter perivascular spaces: an MRI marker in pathology-proven cerebral amyloid angiopathy? Neurology 82(1): 57–62
11. Charidimou A, Pantoni L, Love S (2016) The concept of sporadic cerebral small vessel disease: A road map on key definitions and current concepts. Int. J. Stroke 11(1): 6–18
12. Benedictus MR, Goos JD, Binnewijzend MA et al. (2013) Specific risk factors for microbleeds and white matter hyperintensities in Alzheimer's disease. Neurobiol. Aging 34(11): 2488–2494
13. Biffi A, Anderson CD, Battey TW et al. (2015) Association Between Blood Pressure Control and Risk of Recurrent Intracerebral Hemorrhage. JAMA 314(9): 904–912
14. Charidimou A, Boulouis G, Haley K et al. (2016) White matter hyperintensity patterns in cerebral amyloid angiopathy and hypertensive arteriopathy. Neurology 86(6): 505–511
15. Park JH, Seo SW, Kim C et al. (2013) Pathogenesis of cerebral microbleeds: In vivo imaging of amyloid and subcortical ischemic small

vessel disease in 226 individuals with cognitive impairment. Ann. Neurol. 73(5): 584–593
16. Weller RO, Hawkes CA, Kalaria RN et al. (2015) White matter changes in dementia: role of impaired drainage of interstitial fluid. Brain Pathol. 25(1): 63–78
17. Grinberg LT, Korczyn AD, Heinsen H (2012) Cerebral amyloid angiopathy impact on endothelium. Exp. Gerontol. 47(11): 838–842
18. Schreiber S, Bueche CZ, Garz C et al. (2013) Blood brain barrier breakdown as the starting point of cerebral small vessel disease? - New insights from a rat model. Exp. Transl. Stroke Med. 5(1): 4
19. Purushothuman S, Marotte L, Stowe S et al. (2013) The response of cerebral cortex to haemorrhagic damage: experimental evidence from a penetrating injury model. PLoS. One. 8(3): e59740
20. Hawkes CA, Gatherer M, Sharp MM et al. (2013) Regional differences in the morphological and functional effects of aging on cerebral basement membranes and perivascular drainage of amyloid-beta from the mouse brain. Aging Cell 12(2): 224–236
21. Bueche CZ, Garz C, Stanaszek L et al. (2014) Impact of N-Acetylcysteine on cerebral amyloid-beta plaques and kidney damage in spontaneously hypertensive stroke-prone rats. J. Alzheimers. Dis. 42 Suppl 3: S305-S313
22. Schreiber S, Bueche CZ, Garz C et al. (2012) The pathologic cascade of cerebrovascular lesions in SHRSP: is erythrocyte accumulation an early phase? J. Cereb. Blood Flow Metab 32(2): 278–290
23. Villringer A, Them A, Lindauer U et al. (1994) Capillary perfusion of the rat brain cortex. An in vivo confocal microscopy study. Circ. Res. 75(1): 55–62
24. Berezin V, Walmod PS, Filippov M, Dityatev A. Targeting of ECM molecules and their metabolizing enzymes and receptors for the treatment of CNS diseases. Progress in Brain Research. 214: 353-88
25. Nedergaard M (2013) Neuroscience. Garbage truck of the brain. Science 340(6140): 1529–1530
26. Tarasoff-Conway JM, Carare RO, Osorio RS et al. (2015) Clearance systems in the brain-implications for Alzheimer disease. Nat. Rev. Neurol. 11(8): 457–470
27. Weller RO, Boche D, Nicoll JAR (2009) Microvasculature changes and cerebral amyloid angiopathy in Alzheimer's disease and their potential impact on therapy. Acta Neuropathol. 118: 87–102
28. Bailey EL, Smith C, Sudlow CL et al. (2011) Is the spontaneously hypertensive stroke prone rat a pertinent model of sub cortical ischemic stroke? A systematic review. Int. J. Stroke 6(5): 434–444
29. Hazama F, Ozaki T, Amano S (1979) Scanning electron microscopic study of endothelial cells of cerebral arteries from spontaneously hypertensive rats. Stroke 10(3): 245-52
30. Fujiwara T, Kondo M, Tabei R (1990) Morphological changes in cerebral vascular smooth muscle cells in stroke-prone spontaneously hypertensive rats (SHRSP). A scanning and transmission electron microscopic study. Virchows Arch B Cell Pathol Incl Mol Pathol 58(5): 377-82
31. Fredriksson K, Nordborg C, Kalimo H et al. (1988) Cerebral microangiopathy in stroke-prone spontaneously hypertensive rats. An

immunohistochemical and ultrastructural study. Acta Neuropathol. 75(3): 241–252
32. Amano S (1977) Vascular changes in the brain of spontaneously hypertensive rats: hyaline and fibrinoid degeneration. J. Pathol. 121(2): 119–128
33. Bailey EL, Wardlaw JM, Graham D et al. (2011) Cerebral small vessel endothelial structural changes predate hypertension in stroke-prone spontaneously hypertensive rats: a blinded, controlled immunohistochemical study of 5- to 21-week-old rats. Neuropathol Appl Neurobiol 37(7): 711-26
34. Ritz M-F, Fluri F, Engelter ST et al. (2009) Cortical and putamen age-related changes in the microvessel density and astrocyte deficiency in spontaneously hypertensive and stroke-prone spontaneously hypertensive rats. Curr Neurovasc Res 6(4): 279–287
35. Fujita Y, Lin JX, Takahashi R et al. (2008) Cilostazol alleviates cerebral small-vessel pathology and white-matter lesions in stroke-prone spontaneously hypertensive rats. Brain Res. 1203: 170–176
36. Simpkins AN, Rudic RD, Schreihofer DA et al. (2009) Soluble epoxide inhibition is protective against cerebral ischemia via vascular and neural protection. Am. J. Pathol. 174(6): 2086–2095
37. Hou H, Zhang G, Wang H, et al. (2014) High matrix metalloproteinase-9 expression induces angiogenesis and basement membrane degradation in stroke-prone spontaneously hypertensive rats after cerebral infarction. Neural Regen Res. 2014;9(11): 1154-1162
38. Carnevale D, Mascio G, D'Andrea I et al. (2012) Hypertension induces brain beta-amyloid accumulation, cognitive impairment, and memory deterioration through activation of receptor for advanced glycation end products in brain vasculature. Hypertension 60(1): 188–197
39. Carnevale D, Perrotta M, Lembo G et al. (2016) Pathophysiological Links Among Hypertension and Alzheimer's Disease. High Blood Press Cardiovasc. Prev. 23(1): 3–7
40. Gentile MT, Poulet R, Di Pardo A et al. (2009) Beta-amyloid deposition in brain is enhanced in mouse models of arterial hypertension. Neurobiol. Aging 30(2): 222–228
41. Hutchings M, Weller RO (1986) Anatomical relationships of the pia mater to cerebral blood vessels in man. J. Neurosurg. 65(3): 316–325
42. Attems J, Jellinger K, Thal DR et al. (2011) Review: sporadic cerebral amyloid angiopathy. Neuropathol. Appl. Neurobiol. 37(1): 75–93

Figure legends

Figure 1. Immunocytochemical and morphological basement membrane changes in small vessels in SHRSP and Wistar controls. Graphs demonstrate the collagen IV relative % signal area of the sum of small vessels with a luminal diameter ≥ 15µm and < 15µm (**A**), of vessels with a luminal diameter ≥ 15µm (**B**), and of vessels with a luminal diameter < 15µm (**C**), separately for cortical regions, striatum and thalamus in Wistar rats and SHRSP. In arterioles/small arteries (luminal diameter ≥ 15µm), there was a significant increase of the cortical, striatal and thalamic collagen IV relative % signal area in SHRSP compared to Wistar controls (**B**).

Age had a significant impact on striatal, thalamic and hippocampal basement membrane thickness as measured by transmission electron microscopy (TEM) in SHRSP (**D**), but not in Wistar rats (**E**). TEM basement membrane thickness was moreover significantly increased in the striatum, the thalamus and the hippocampus in SHRSP compared to Wistar rats (**F**).

Error bars indicate the 95% CI, ** $p \leq 0.01$. **A-C**, SHRSP n = 15 (18 to 32 weeks), Wistar n = 15 (18 to 32 weeks), **D-F**, SHRSP n = 9 (18 to 32 weeks), Wistar n = 9 (18 to 32 weeks)

Figure 2. **Collagen IV positive small vessels in SHRSP and Wistar rats.** Figure demonstrates the collagen IV relative % signal area in cortical (**A, B**), striatal (**C, D**) and thalamic (**E, F**) regions in male SHRSP (**A, C, E**) and Wistar controls (**B, D, F**). Larger vessels (luminal diameter ≥ 15µm) had a visibly increased collagen IV relative % signal area in SHRSP versus controls.

Figure 3. Ultrastructural cortical basement membrane changes in SHRSP. Ultrastructural changes in 24-32 week SHRSP brains, with arrowheads pointing to: (**A**) dissociation of astrocytic end feet from the basement membrane and ruffling to the edge of the basement membrane, (**B**) accumulation of lipofuscin in pericytes, (**C**) accumulation of fibrillary structures in the basement membrane, (**D**) the swollen basement membrane

containing electron dense deposits, (**E**) an increase in the number and size of the caveolae in pericytes, endothelial cells and the (**F**) folding of the tight junctions.

Figure 4. Regional incidence of CAA findings. Regional color-coding reflects the incidence with which Aβ-positive vessels in the respective regions were found in the SHRSP. Color coding is overlaid on axial slices of grey and white matter segments of a T2-weighted MRI scan of a rat brain (own unpublished data) and rendered onto its surface.

Figure 5. Cerebral amyloid angiopathy in SHRSP. SHRSP spontaneously develop cerebral amyloid angiopathy (**A-E**, arrows), found in capillaries (**a1, b2, b3, c1, d2**, arrows), and in smaller and bigger arterioles/small arteries (**a2, b1, c2, c3, d1, e1**, arrows). Endogenous amyloid-β (Aβ) accumulates initially on the abluminal side of the vessel walls (**D-E**, arrows), with additionally diffuse and sparse amyloid accumulations in the vessel wall elements (**E, e1**), and extending eccentrically from the vessel wall of small arterioles into the perivascular parenchyma (dysphoric angiopathy; **F, f1-f2**, arrows).

STL - solanum tuberosum lectin-fluorescein isothiocyanate (endothelial marker), DAPI - 4'.6-diamidino-2-phenylindole (nuclear staining), **A, a1, a2, F, f1, f2** – Prussian blue/CR-staining, **B, b1, b3, C, c1-c3** – Prussian blue/Thioflavin T-staining, **b2** – Prussian blue/Thioflavin S-staining, **D, d1, d2, E, e1** – Immunohistochemistry for Aβ/Alexa555, **A, a1, B, b1, b3** – 18 weeks (w), **a2, b2, C, c1, c2, D, d1, d2, E, e1, f2** – 32 w; **c3, F, f1** – 32 w

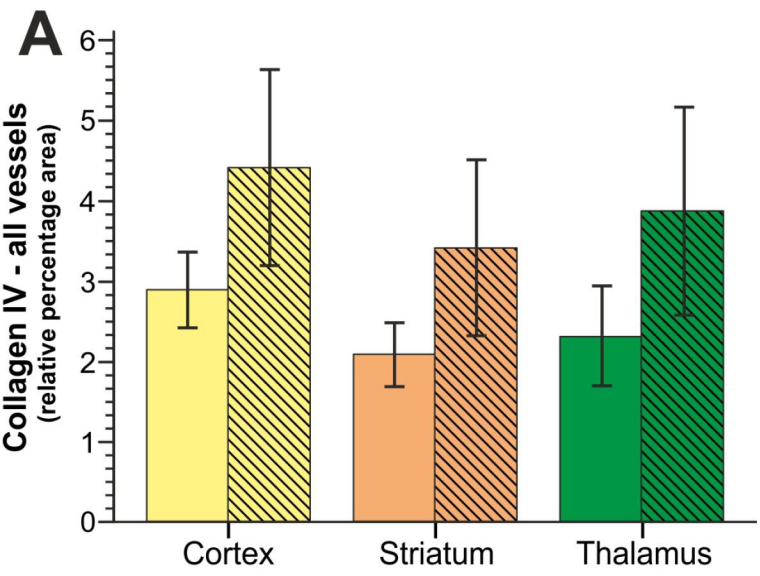
A
Collagen IV - all vessels
(relative percentage area)
0
1
2
3
4
5
6
Cortex
Striatum
Thalamus

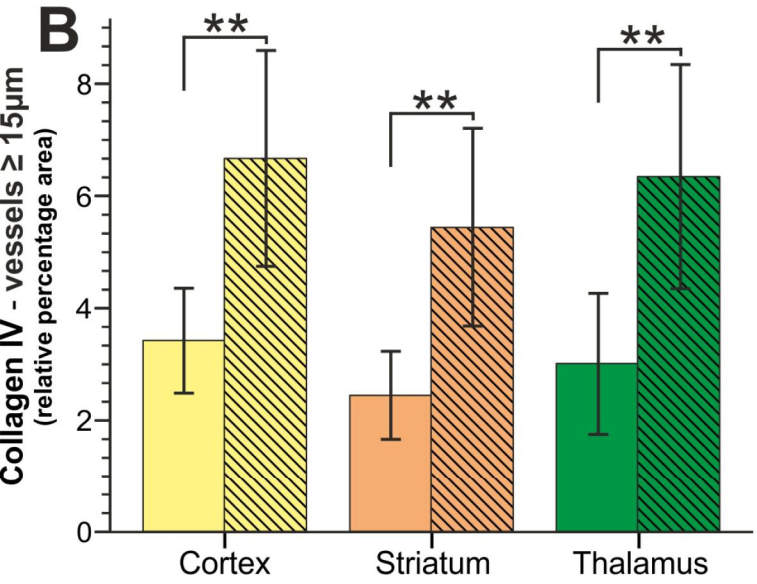
B
Collagen IV - vessels ≥ 15µm
(relative percentage area)
0
2
4
6
8
**
**
**
Cortex
Striatum
Thalamus

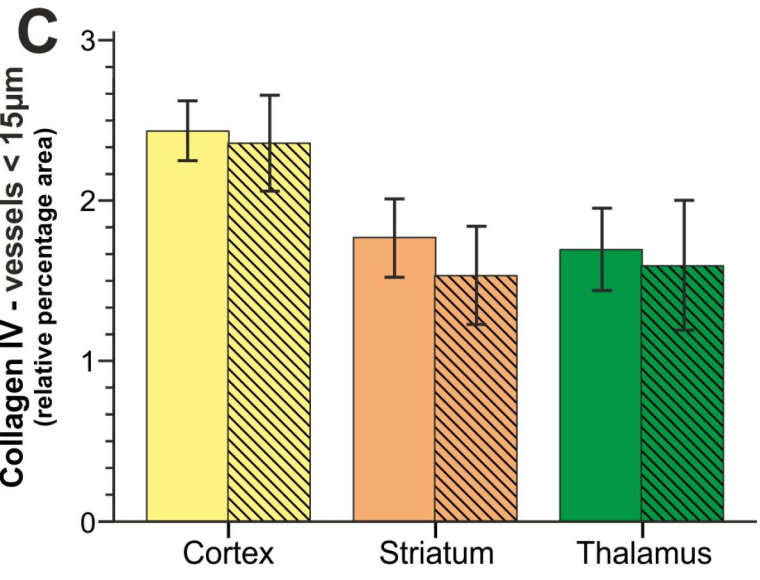
C
Collagen IV - vessels < 15µm
(relative percentage area)
0
1
2
3
Cortex
Striatum
Thalamus

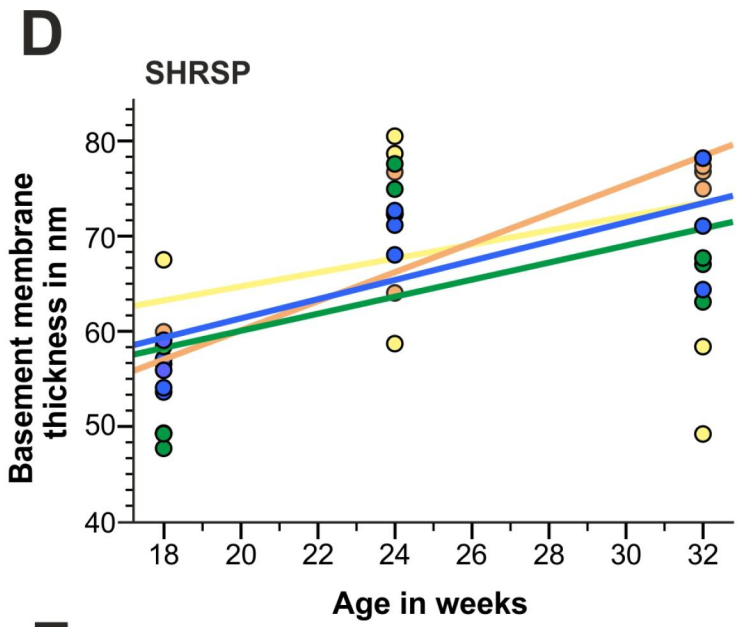
D
SHRSP
Basement membrane thickness in nm
40
50
60
70
80
18
20
22
24
26
28
30
32
Age in weeks

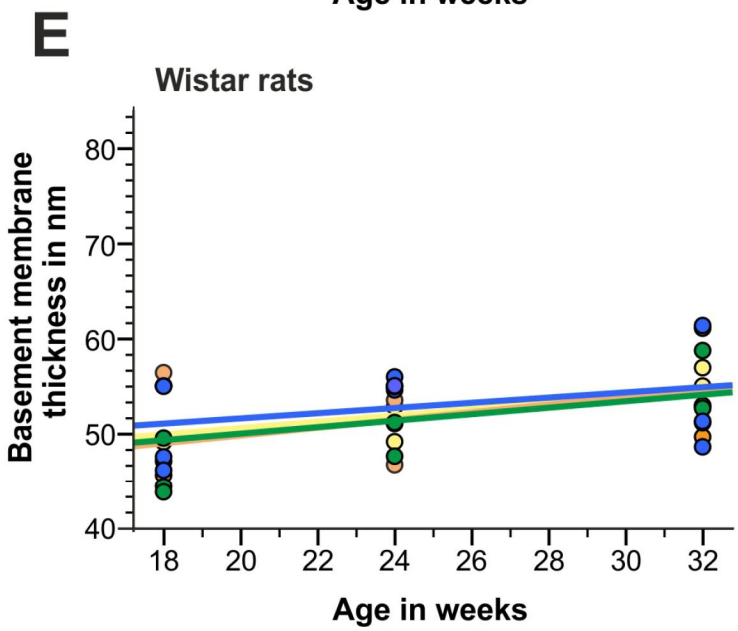
E
Wistar rats
Basement membrane thickness in nm
40
50
60
70
80
18
20
22
24
26
28
30
32
Age in weeks

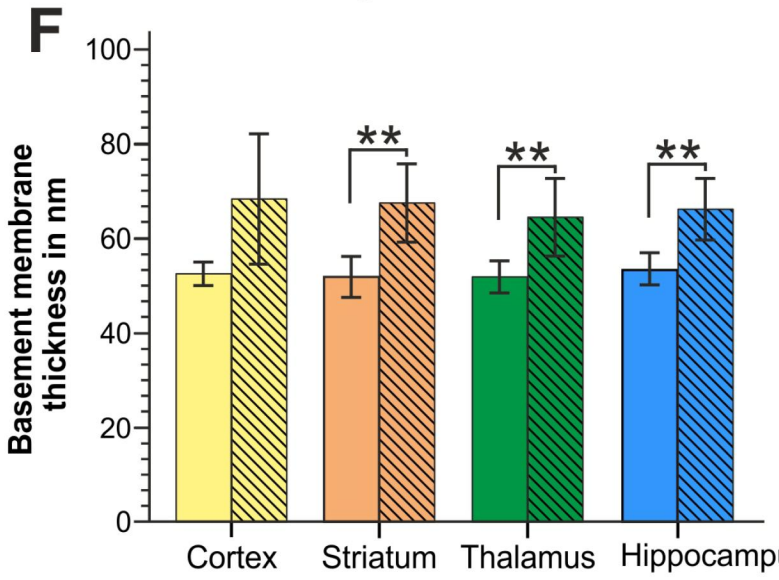
F
Basement membrane thickness in nm
0
20
40
60
80
100
**
**
**
Cortex
Striatum
Thalamus
Hippocampus


Cortex
Striatum
Thalamus
Hippocampus
Wistar rats
SHRSP

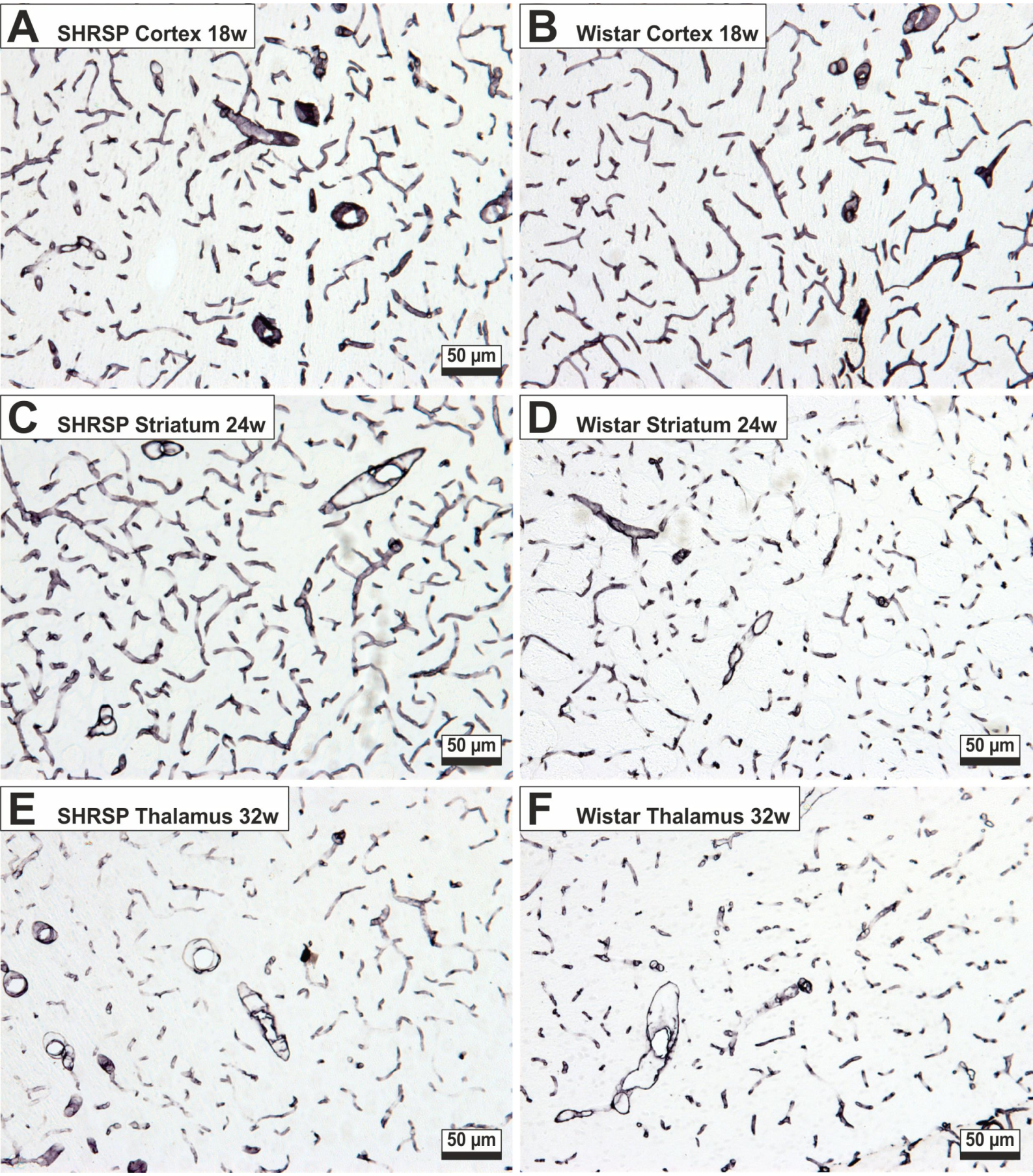
A SHRSP Cortex 18w
50 µm
B Wistar Cortex 18w
C SHRSP Striatum 24w
50 µm
D Wistar Striatum 24w
50 µm
E SHRSP Thalamus 32w
50 µm
F Wistar Thalamus 32w
50 µm

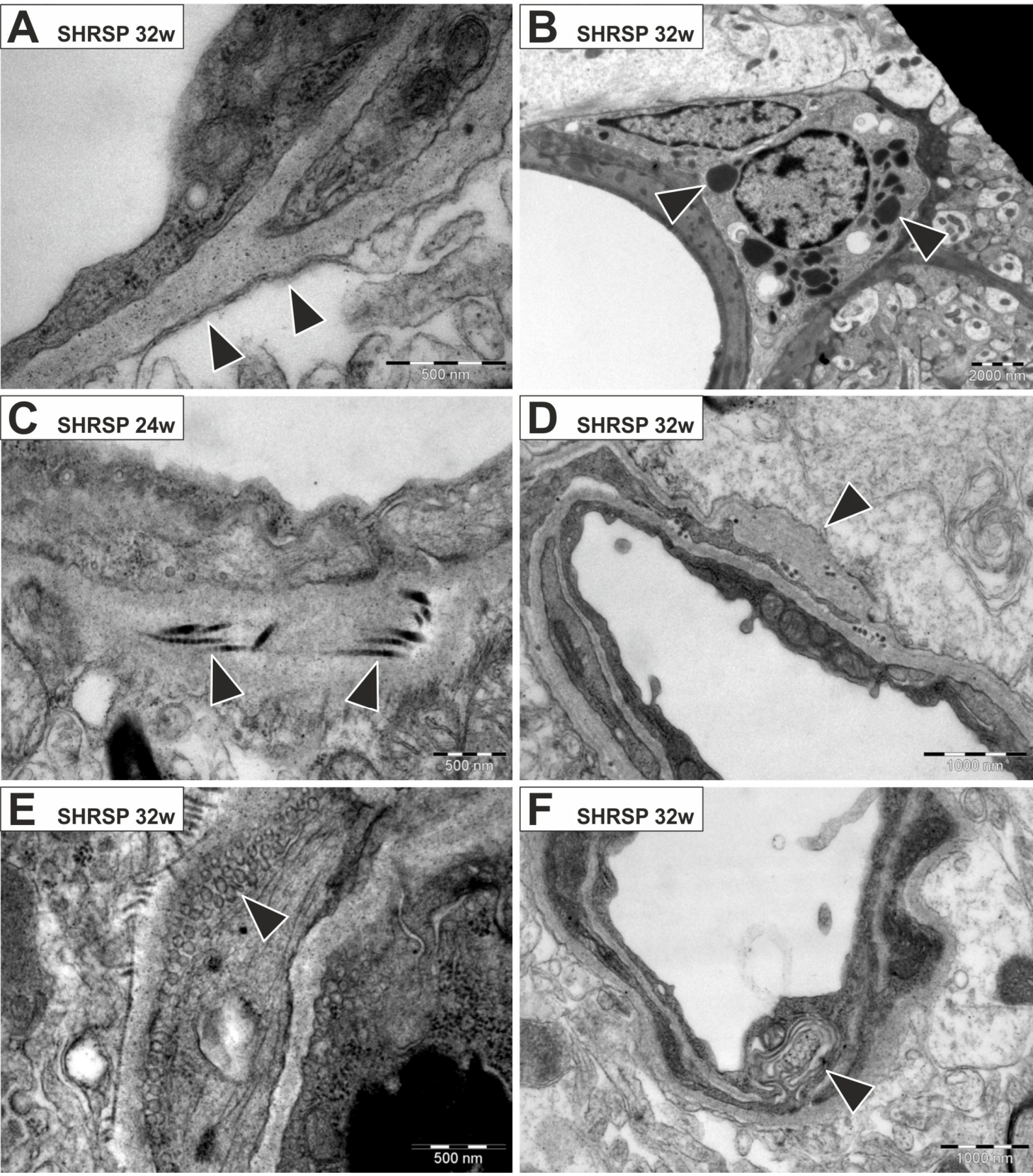
A SHRSP 32w
500 nm
B SHRSP 32w
2000 nm
C SHRSP 24w
500 nm
D SHRSP 32w
1000 nm
E SHRSP 32w
500 nm
F SHRSP 32w
1000 nm

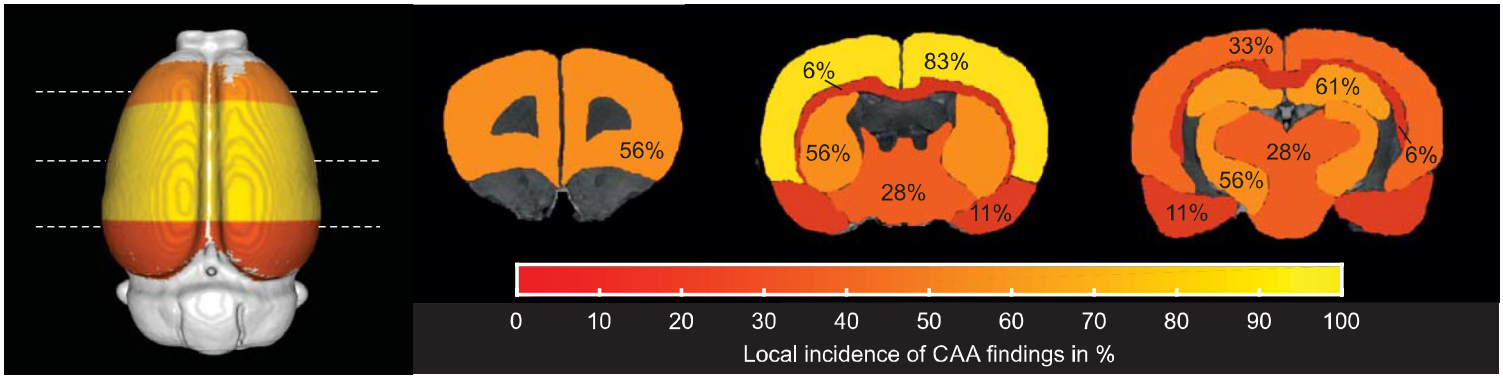
56%
6%
83%
56%
28%
11%
33%
61%
28%
6%
56%
11%
0
10
20
30
40
50
60
70
80
90
100
Local incidence of CAA findings in %

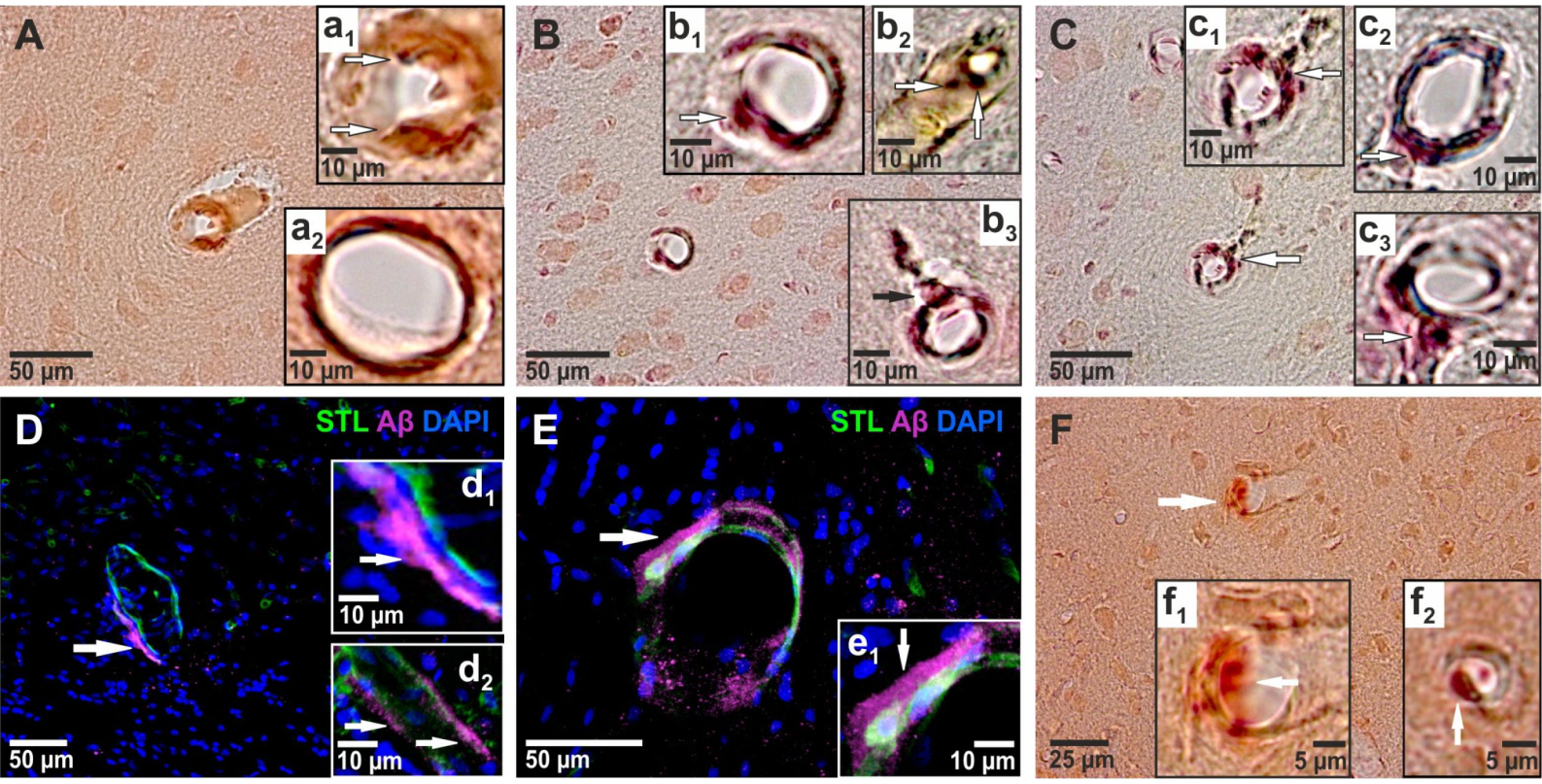
A
a1
10 μm
a2
10 μm
50 μm
B
b1
10 μm
b2
10 μm
b3
10 μm
50 μm
C
c1
10 μm
c2
10 μm
c3
10 μm
50 μm
D
STL Aβ DAPI
d1
10 μm
d2
10 μm
50 μm
E
STL Aβ DAPI
e1
10 μm
50 μm
F
f1
5 μm
f2
5 μm
25 μm